Eurasian Journal of Biological and Chemical Sciences

Tamoxifen Delivery to Breast Cancer Cells (MCF-7) Via Hydroxyapatite Microspheres

Binnaz Kırbıyık[1], Birgül Mazmanci[1,2] , Şeyma Gülnaz Yarlilar[1*] , Naz Uğur[3], Kasım Ocakoğlu[3]

[1] *Department of Nanotechnology and Advanced Material, Science Institute, Mersin University, 33363, Mersin, Turkey.*
[2] *Department of Biology, Faculty of Science and Letter, Mersin University, 33363 Mersin, Turkey.*
[3] *Department of Engineering Fundamental Sciences, Faculty of Engineering, Tarsus University, 33400, Tarsus, Turkey*

*Corresponding author : syarlilar@gmail.com
Orcid No: https://orcid.org/0000-0002-0403-3390

Abstract: Drug delivery systems have been used in cancer treatment to increase drug effectiveness. The hydroxyapatite (HAP) based materials used in this area can provide drug transport to the target site without its deterioration. In this study, porous hollow hydroxyapatite microspheres (PHHMs) were produced by using the hydrothermal method. Tamoxifen (TAM) used in the treatment of breast cancer has been covalently attached to the produced microspheres. The obtained microsphere structures (tamoxifen-loaded hydroxyapatite, TAM/H) were successfully characterized by ATR-FTIR, FE-SEM, XRD, and DLS methods. The breast cancer cell line MCF-7 was used to examine the effect of the hybrid structure. The cytotoxic and genotoxic effects of TAM/H were compared with the TAM groups on MCF-7. Our results have showed that, the decrease in cell viability at 24 and 36 hours were still continued at 48 hours only in TAM/H groups. In addition, TAM/H was found to show a genotoxic effect by the increment in genetic damage index (GDI) and damaged cell percentage (DCP%). As a result, use of hydroxyapatite was suitable for the transport of TAM and that covalent binding was suitable for drug particle interaction with hybrid structure and thus controlled drug release occurred.

Keywords: Hydroxyapatite microsphere, Tamoxifen, Hydrothermal method, MCF-7, Cytotoxicity, Genotoxicity.

1. Introduction

Cancer and cancer treatment are a weighty matter in our century. Among other cancer types, breast and lung cancer has been reported to be the most common types (Greenlee et al. 2001). In the medical field, surgery and drug therapy are the leading processes for the treatment of cancer. These methods rely on the removal of the cancerous cells. In chemotherapy, cancer cells are aimed to be annihilated by anti-cancer drugs. Anti-cancer drugs are nonselective and can also damage healthy normal tissues, causing severe side effects such as loss of appetite and nausea. These side effects induced by chemotherapeutic drugs on healthy tissues and organs are a major reason behind the high mortality rate of cancer patients (Senapati et al. 2018).

The side effect of conventional chemotherapy have led to the development of nanoparticle-based drug delivery systems (Yao et al. 2020). Nanoparticle-based drug applications have emerged as promising tools to eliminate the pharmacokinetic interaction associated with traditional drug formulations (Blanco et al. 2015). Commonly used drug carriers are polymeric dendrimers, micelles, microspheres, liposomes, quantum dots, nanoemulsions, gold nanoparticles, and hydrogels (Singh et al. 2017). Nanoparticles for drug delivery include numerous designs in size, shape, and material. Each nanoparticle differs in drug loading capacity, particle and drug stability, drug release rates, and targeted release ability (Haley et al. 2008). Nanoparticles can increase the intracellular concentration of drugs in cancer cells while preventing toxicity in normal cells, using both passive and active target strategies. Besides, the surfaces of the nanoparticles are activated with a higher degree of affinity for cancer cells to bind to cancer cells, rather than healthy cells. Thus, drug concentrations in cancer cells are increased with the effect of nanoparticles, while the undesirable toxic effect that can occur in healthy cells can be minimized (Maeda et al. 2000; Allen et al. 2002).

Today, the production of nanostructured bioceramics and their applications in biomedical fields have become important. Hydroxyapatite (HAP), a bioceramic species, is widely used in different scientific fields such as tissue engineering, drug delivery systems, and chromatographic purification (Jafari et al. 2014). It is a remarkable element of the bioceramics group due to its structural similarity to

the mineral structure of bones and teeth. Because of their good bioactivity and biocompatibility, hydroxyapatite participates in the solid-fluid balance in the environment in which they are placed. In addition, they can directly connect with the bone and other hard tissues and muscles where they are placed (Hench et al. 1993; Pasinli 2004). The reason is that their porous structures offer a high binding affinity for various pharmacological agents such as antibiotics, hormones, enzymes, antibody fragments, steroids (Netz et al. 2001). Concurrently, HAP protects the drug from spoilage until it reaches the physical or chemical target area. At the same time, controlled drug release occurs gradually. Therefore, bioceramics are excellent candidates as promising bio-scaffolds in targeted drug release and tissue engineering (Uskokovic et al. 2014; Andres et al. 2018).

Tamoxifen (TAM) is the most commonly used anti-estrogen drug to treat advanced and early breast cancer and reduce the incidence of breast cancer in high-risk women (Paganini et al. 2000). The drug is classified as a selective estrogen receptor modulator because it is an estrogen agonist/antagonist that alters hormone action by competing with estrogen to bind to the estrogen receptor and partially blocking the endogenous estrogen effect (Bender et al. 2007). Due to its anti-estrogenic effects, TAM was originally used to treat estrogen receptor-positive breast cancers. Nevertheless, TAM (20 mg/day) used in studies to treat breast cancer was shown to inhibit the growth of breast cancer cells (Carlson et al. 2006). Later, the use of the drug was developed to include all types of breast cancer, and more recently it was also used in the prevention of breast cancer for healthy women at high risk (Fisher et al. 1998).

In this study, porous hollow hydroxyapatite microspheres (PHHMs) are successfully synthesized by a hydrothermal method and TAM was covalently bonded to PHHMs. TAM loaded hydroxyapatite microspheres (TAM/H) were obtained. Chemical compositions and properties of TAM/H are determined by Attenuated Total Reflectance-Fourier Transform Infrared Spectroscopy (ATR-FTIR), Field Emission Scanning Electron Microscopy (FE-SEM), X-ray diffraction (XRD), and Dynamic Light Scattering (DLS). In addition, the cytotoxicity and genotoxicity were also explored for bioactivity of TAM/H. A comparison with only TAM was made to test the availability of HAP microspheres in drug delivery.

2. Materials and Methods
2.1. Material
Fetal bovine serum, penicillin-streptomycin, trypsin-EDTA solution, L-glutamine 100X 200mM-100mL were bought from Biowest. Ethylene dinitro tetra acetic acid (EDTA), trizma hydrochloride, ethidium bromide, agarose, agarose-low gelling temperature, trypan blue, poly(sodium 4-styrenesulfonate) (PSS, $M_w \sim 16800$), calcium chloride, sodium carbonate, disodium hydrogen phosphate, hydrochloric acid were purchased from Sigma-Aldrich. Dimethyl sulfoxide, sodium hydroxide, sodium chloride, triton X-100 were purchased from Merck. All reagents were used without further purification.

2.2 Methods
2.2.1 Synthesis of tamoxifen-loaded hydroxyapatite (TAM/H) microspheres
For a typical synthesis of porous hollow hydroxyapatite microspheres (PHHMs), a previously reported hydrothermal method by Wen Lai and co. workers (Lai et al. 2016) was carried out. Briefly, $CaCO_3$ (vaterite) was synthesized as the first step. For the synthesis of vaterite, 10 mL $CaCl_2$ (0.2 M) solution was mixed with 100 mL PSS and stirred under room temperature with a magnetic stirrer. Subsequently, 10 mL Na_2CO_3 (0.2 M) was added to the solution dropwise and continued to stir for 1 h. The white $CaCO_3$ suspension was washed with ethanol and distilled water, dried in the 60 °C oven for 24 h. 0.2 g vaterite and 0.1 M Na_2HPO_4 were mixed, and NaOH was added until pH 11. Then, the transparent suspension was transferred to Teflon autoclave and hydrothermal reaction continued for 120 °C, 1 h. After the reaction, the obtained porous hollow hydroxyapatite microspheres were centrifuged and washed with absolute ethanol and distilled water then dried in the 60 °C oven for 24 h.

Complex hybrid structures of TAM/H were obtained by integration of TAM to the synthesized porous hollow hydroxyapatite microspheres. The covalent bonding method was applied in the formation of the complex structure. Hybrid structures synthesized at each step have shown in Figure 1.

At the first part (Step 1), 300 mg PHHM was dissolved in 3 mL dry toluene in an inert atmosphere and stirred with a magnetic stirrer at 70 °C. Then, 0.9 mL Triethoxy-3-(2-imidazolin-1-yl)propylsilane was added to the solution and stirred for 24 h. Obtained structure was named PHHM/Si.

At the second step (Step 2), 1.5 mL 1,4-diiodobutane was added to the solution and continued to stir for 24 h in the dark. After, the reaction mixture was filtered and washed five times with diethyl ether. Then, the solid was dried in RT for 48 h in the dark. Obtained structure was named PHHM/SiI. At the third step (Step 3), 50 mg of PHHM/SiI was dissolved in 2 mL dry toluene in an inert atmosphere and stirred with a magnetic stirrer at 90 °C. Then, 100 mg TAM was dissolved in 2 mL dry toluene thereafter, added to the reaction, and continued to stir for 48 h. After the reaction, the obtained material was washed several times with diethyl ether. After, the solid was dried in RT for 48 h in the dark. The final structure was named as TAM/H.
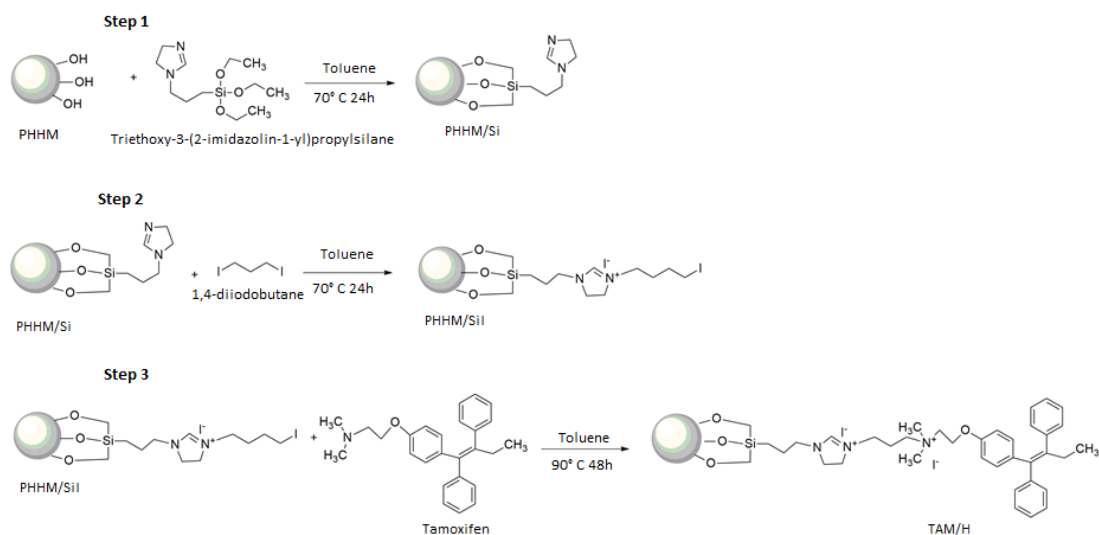
Fig. 1 TAM/H hybrid structure synthesis steps

2.2.2. Characterization

The surface morphology and microstructure of the vaterite and PHHM structures were examined by field emission scanning electron microscopy (FE-SEM, JEOL JSM-6060LV). The structural properties of PHHM were analyzed with a Cu-Kα welded X-ray diffractometer (Bruker D8 Advanced Series) at a scanning rate of 5 ° min^{-1} at wavelength λ = 1.54056 Å, in the range 20-60º. The functional groups in the vaterite, PHHM, PHHM / SiI, TAM structures, the TAM/H microsphere structures were determined by ATR-FTIR (Perkin Elmer Spectrum Two Model). FTIR spectra were collected at room temperature in the 4000-450 cm^{-1} wavelength range.

2.2.3. Bioactivity of TAM/H microspheres

2.2.3.1. Cell culture and treatment

The bioactivity of TAM/H was investigated via cell viability and genotoxicity tests. For this purpose, the human breast cancer cell line MCF-7 was preferred. The breast cancer cell line MCF-7 was obtained from Mersin University, Advanced Technology Laboratory, Turkey.

2.2.3.2. Cell viability testing

Cell viability analysis was performed by xCELLigence system. The xCELLigence system allows for label-free and dynamic monitoring of cellular phenotypic changes in real-time using impedance. Increasing the number of adherent cells and changing conditions in the cell culture alter the impedance. The impedance gives quantitative information about the number, viability, morphology, and migration of the cells (Garcia et al. 2013; Şener et al. 2017).

The cells were placed into tissue culture flasks under humidified 5% CO$_2$ and 95% air maintained at 37 °C atmosphere in Dulbecco's modified Eagle's medium (DMEM) supplemented with 10% fetal bovine serum (FBS, v/v), 1% penicillin (100 U/ml)-streptomycin (100 mg/ml) and 1% glutamine (100 mg/ml). MCF-7 cells were passaged with 0.25% trypsin and 0.1% ethylene diamine tetraacetic acid (EDTA) after 80% confluency. After seeding 200 μl of the cell suspensions in DMEM containing 10% FBS into the wells (10.000 cells/well) of the E-plate 16. Cells were allowed to adhere to the E-plate for 24 h and subsequently, the media was removed from the well. The cells were treated with different doses (10, 20, 40, 60 μM) of TAM/H. To demonstrate the effectiveness of TAM/H in MCF-7 cells, free tamoxifen (TAM) groups were performed using the same doses of tamoxifen (10, 20, 60 μM). Only the medium was added to the control group (CONT). The changes in the MCF-7 cell proliferation were monitored every 15 min for 92 hours by xCELLigence device. Cell proliferation experiments were performed in triplicate.

2.2.3.3. Comet assay

The comet assay is a single-cell gel electrophoresis method used as a genotoxicity test for measuring DNA damage (Tice et al. 2000). MCF-7 cells were seeded in the tissue-culture plates (2 x 10^5) and incubated for 48h for the cell attachment and subsequently, 4h, the cells were treated with different doses (10, 20, 40, 60 μM) of TAM/H microspheres and different doses (10, 20, 40, 60 μM) of free Tamoxifen (TAM). Cells were harvested by trypsin –EDTA solution. After, washed with PBS and resuspended in ice-cold PBS. About 40 μL of the resuspended cells was mixed with 250 μL of low melting point agarose at 37 °C. Afterward, 100 μL suspension was spread evenly onto a slide. The slides were placed at 4 °C in the dark until gelling had occurred. In the sequel, immersed in chilled lysis buffer at 4 °C for 60 min. After lysis and unwinding, the slides were placed in an electrophoresis tank filled with alkaline electrophoresis buffer. The electrophoresis runs for 20 min at 35 V and 300 mA. After electrophoresis, the slides were transferred into chilled neutralization buffer for 10 min and cold 70% ethanol for 5 min. Thereafter, the slides were air-dried overnight at room temperature and then stained with Ethidium Bromide. The DNA migration was observed using a fluorescence microscope (BX51, Olympus, Tokyo, Japan). H$_2$O$_2$ solution was used as a positive

control. For each concentration, 100 randomly selected cells were analyzed. The results were given as Arbitrary Units (AU) values which were used to express the DNA damage. AU values indicating the comet assay results were as: Undamaged, (Type 0); low-level damaged (Type 1); moderately damaged (Type 2); highly damaged (Type 3); ultrahigh-level damaged (Type 4). Two parameters were calculated as genetic damage index (GDI) and damaged cell percent (DCP%) (Çavaş 2011).

2.2.3.4. Statistical analysis

All bioactivity studies were carried out in triplicate and results were expressed as means ± SD. Statistical significance between groups was evaluated using Tukey-HSD for post-hoc multiple comparisons. $p < 0.05$ was considered statistically significant.

3. Results and discussion

3.1. Characterization of Vaterite, PHHM, PHHM/SiI and TAM/H microspheres

The size and morphology of the hydroxyapatite structures were characterized by FESEM and Dynamic Light Scattering (DLS) methods. SEM images of synthesized vaterite ($CaCO_3$) and PHHM are shown in Figure 2a and b. As seen from the SEM images; vaterite structures were obtained in spheres and homogenously dispersed with an average dimension size of around 1000 nm, and this is in line with the results previously reported in the literature (Lai et al. 2016). PHHM was obtained in the form of mesoporous and hollow microspheres with a uniform morphology (Figure 2c and d). The images also revealed that their dimensions are bigger than that of vaterite structures (Lai et al. 2016). According to DLS measurements, it was determined that the particle size distribution of PHHM is between 0.8 - 2.0 μm, and the average diameter is about 1.2 μm (Figure 2e) (Lai et al. 2016). The obtained data were also compatible with SEM analysis.

The XRD pattern of the PHHM structure was shown in Figure 3. The reflections match the characteristic diffraction peaks of the hexagonal hydroxyapatite (JCPDS No. 09-0432). However, the weak calcium carbonate ($CaCO_3$) and calcium hydroxide $Ca(OH)_2$ peaks are seen in the 27-30° range. The calcium carbonate particles were formed by the reaction of the increased calcium hydroxide due to the acidic conditions of hydroxyapatite synthesis with atmospheric carbon dioxide.

An understanding of the surface properties of the synthesized vaterite ($CaCO_3$), PHHM, PHHM/SiI and TAM/H microstructures requires precise characterization of the associated structures. At this point, FTIR spectroscopy which provides important information about surface properties was firstly used. The IR spectrum of the synthesized vaterite was measured between 450-4000 cm^{-1} (Figure 4a). Two absorption bands at 927 cm^{-1} and 798 cm^{-1} and a high level between 1507-1454 cm^{-1} are indicating carbonate (CO_3^{-2}) groups (Wu et al. 2010).

The vibrations of 1021 cm^{-1}, 1414 cm^{-1} and the absorption bands at 562 cm^{-1} and 602 cm^{-1} belonging to the bending vibrations of the phosphate (PO_4^{-3}, P = O) groups of PHHM structures (Figure 4b) (Rocha et al. 2005; Rehman et al. 2016; Taşkın et al. 2018). Besides, the peaks at 872 cm^{-1}, 1414 $cm^{-1,}$ and 1465 cm^{-1} are considered to have a high level of B-type CO_3^{-2} absorption so that CO_3^{-2} is included in the lattice structure (Lai et al. 2016).

Tamoxifen's (TAM) characteristic absorption peaks are shown in Figure 4c. Phenyl ring vibration band (=C-H) at 3027 cm^{-1}; aromatic groups (C=C) at 1556 cm^{-1}, 1521 cm^{-1} and 1460 cm^{-1}; phenyl ring substitution at 770 cm^{-1} and 718 cm^{-1}; methylamine (C-N) at 978 cm^{-1} were characterized (Maji et al. 2014; Nosrati et al. 2017). In Figure 4d, 1655 cm^{-1} peak refers to the -NH strain peaks and the heterocyclic -CH strain p eaks of the imidazole groups in PHHM/SiI structure (Bora et al. 2012; Han et al. 2009). Furthermore, the peak at 502 cm^{-1} is determined to be Si-O strain peak from the silanol group which indicates amine-bonded groups of the silanol groups (Lazarevic et al. 2015). The weak peak at 694 cm^{-1} belongs to C-I vibration band of 1,4-diiodobutane (Simek et al. 2015). The performed characterization studies showed that the complex structure (PHHM/SiI) formed by binding triethoxy-3-(2-imidazolin-1-yl)propylsilane and 1,4-diiodobutane to the PHHM structure was successfully obtained. After the integration of TAM onto the PHHM/SiI complex structure, the vibration bands of TAM representing phenyl ring (C = C) of 1556 cm^{-1} and 1521 cm^{-1} have shifted to 1599 cm^{-1} and 1505 cm^{-1} respectively (Figure 4e). From the obtained data, it was determined that the steps of the covalent bonding of TAM onto the PHHM/SiI structure were successfully carried out.

3.2. Bioactivity

The comparison of cytotoxic effects of TAM/H microspheres and TAM were done in MCF-7 cell line using a real-time cell analyser. As a result of the xCelligence analysis, the time duration / dose interaction was not statistically significant and therefore comparisons were made between dose groups for each time period. The cell index values and percentage cell viability were shown in Table 1.
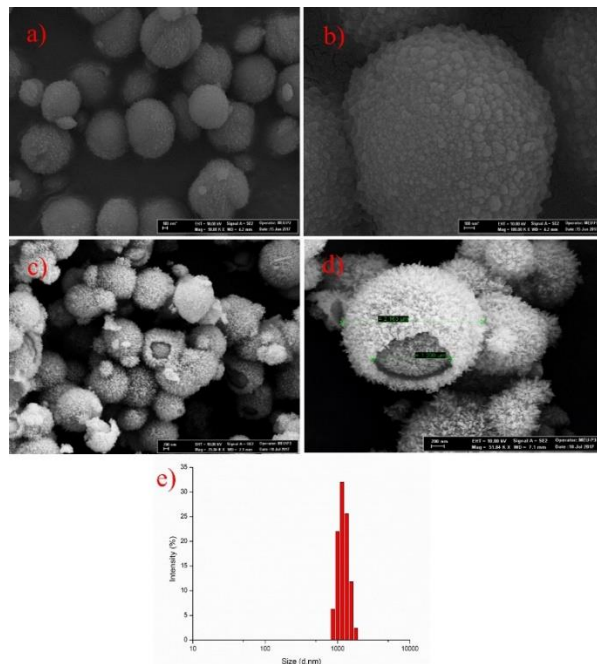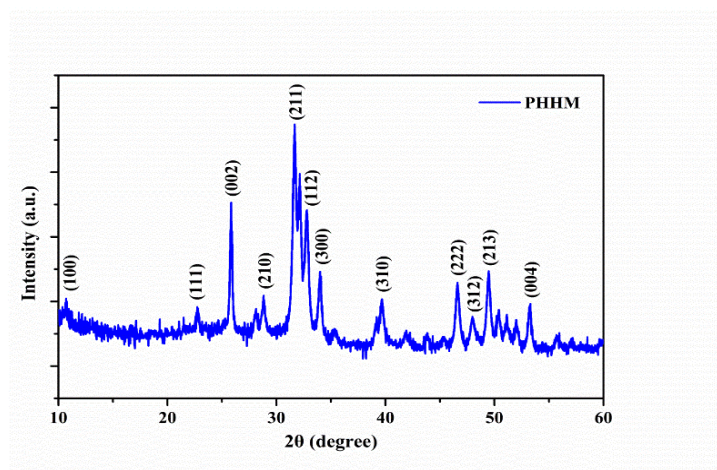
Fig. 2 SEM images of synthesized vaterite (CaCO$_3$) and PHHM

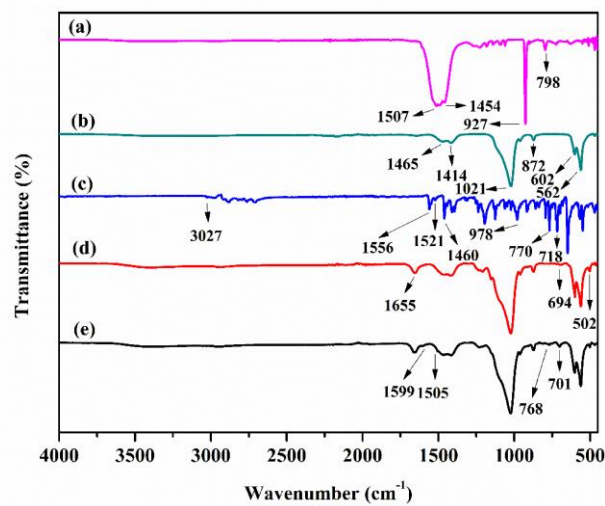**Fig. 3** XRD pattern of the PHHM structure

Fig. 4 FTIR spectrum of the synthesized materials.

Table 1: Cell index and cell viability percentages of control and experimental groups

	12 h		24 h		36 h		48 h	
	Cell index	Cell via. (%)	Cell index	Cell via. (%)	Cell index	Cell via. (%)	Cell index	Cell via. (%)
Control	8.58 ± 0.49	100	10.51 ± 0.36	100	10.74 ± 0.29	100	10.60 ± 0.36	100
TAM/H 10	8.80 ± 0.36	102.6	9.45 ± 0.06	89.9	9.15 ± 0.14	85.2	9.00 ± 0.27*	84.9*
TAM/H 20	8.75 ± 0.32	102.0	9.42 ± 0.13	89.6	9.06 ± 0.22	84.4	8.84 ± 0.16*	83.4*
TAM/H 60	8.27 ± 0.94	96.4	9.40 ± 0.22	89.4	9.60 ± 0.61	89.4	9.20 ± 0.61	86.8
TAM 10	9.41 ± 0.55	109.7	9.95 ± 0.57	94.7	10.31 ± 0.41	96.0	11.10 ± 0.46	104.7
TAM 20	9.64 ± 0.76	112.4	8.56 ± 0.24*	81.4*	9.05 ± 0.78*	84.3*	10.54 ± 0.55	99.4
TAM 60	9.58 ± 0.22	111.7	9.86 ± 0.26	93.8	10.37 ± 0.09	96.6	11.18 ± 0.05	105.5

*significant difference compare to control ($p < 0.05$) Values are given mean ± standard deviation.

At the each time period statistical difference was not found significantly (p>0.05) between TAM and TAM/H groups. When TAM and TAM / H groups were compared with the control group, cell index was decreased approximately 5.3-18.6% for TAM groups and 10.1-10.6% for TAM/H groups with compared to the control in 24th h. At 36th hour, the cell index was decreased by 14.8%, 15.6% and 10.6 in the TAM/H 10, TAM/H 20 and TAM/H 60 groups, respectively. At the same time period, cell viability was found to decrease 15.7% in TAM20 group. Decrease of cell index of TAM/H 10, TAM/H 20 and TAM/H 60 groups was reached 15.1%, 16.6% and 13.2% respectively compared to the control at the 48th hour, while cell viability of TAM groups was increased.

Cell viability is an important toxicity assay parameter and is directly associated with the toxic effects of different agents. The xCELLigence system provides real-time monitoring of cells and based on impedance measurements of adherent cells in vitro. Measurement of the electrical impedance gives an idea about adhesion, proliferation and migration of the cells, and it is expressed as the cell index (CI). The CI reflects the cell viability, cell number, attachment quality and cell morphology (Urcan et al. 2010; Öztürk et al. 2018). It was determined that the doses used in this study, both TAM and TAM/H, were toxic to MCF cells. Hassan et al., 2018 reported that the tamoxifen caused a decrease in cell viability in MCF-7 cells and the decrease was dependent on the cell density and tamoxifen concentration (Hassan et al. 2018). Tamoxifen effect by causing loss of cell membrane integrity, down-regulation of telomerase activity, and change in nuclear morphology (Khadka et al. 2015). As a result, cell viability decreased in TAM/H and TAM groups at 24th and 36th hours, while the decrease continued in TAM/H group and increased

viability in TAM groups at 48th hours. This shows that TAM was released slowly from tamoxifen-loaded microspheres and the effect of TAM in the hybrid structure is long-term and more effective. Previous study with doxorubicin-loaded microspheres, it has been reported that the porous hydroxyapatite microsphere structures are suitable for drug release (Huang et al. 2020). In this study indicates that porous HAP structures and covalent binding of the drug are suitable for prolonged action.

Comet assay results are shown in Table 2. The DCP% significantly increases in all TAM and TAM/H dose groups compared with the negative control group (p < 0.05). Tamoxifen treatment caused DNA damage as well as cytotoxic damage. The maximum increase in the TAM/H and TAM groups is at 20 µM and 40 µM dose, respectively. Increases in DCP% are higher than the PC group. Also, GDI increased in TAM/H and TAM groups compared with the NC group (p≤0.05). Either damaged cell percentage (DCP%) or genetic damage index (GDI) the increase based on the free TAM and TAM/H microspheres. DCP% and GDI values are higher in loaded groups (TAM/H) than free TAM groups. The study conducted by Wozniak. et al (2007), the DNA damage potential of TAM in peripheral blood lymphocytes and MCF-7 breast cancer cells compared using the comet test. In the data obtained, it has been determined that TAM damages DNA in both normal cells and cancer cells and mainly causes DNA strands to break. TAM has been reported to exhibit genotoxic effects in normal and cancer cells with free radical formation (Wozniak et al. 2007). Melo et al. Reported that the genotoxic effect induced by tamoxifen (TAM) in the MCF-7 cell line was caused by oxidative DNA damage (Melo et al. 2013).

In this study, free TAM as well as covalently bonded TAM to porous structures show that it has genotoxic potential. Mondal et. all has been reported that mesoporous HAp nanostructures have excellent prospects in drug delivery applications due to their high surface area and high pore volume (Mondal et al. 2018). Our results have shown that, TAM/H hybrit structure is effective in breast cancer cells. Studies are in progress regarding the loading capacity or reaction efficiency of tamoxifen to hydroxyapatite microspheres, as well as the tamoxifen release profile.

Table 2. Comet assay results damaged cell percentages (%DCP) and genetic damage index (GDI).

	% DCP	GDI
TAM/H 10	25 ± 8.48	0.97 ± 0.15*
TAM/H 20	38.5 ± 2.12*	1.47 ± 0.02*
TAM/H 40	33.5 ± 4.94*	1.23 ± 0.18*
TAM/H 60	37 ± 0*	1.37±0.07*
TAM 10	24 ± 0	0.89 ± 0
TAM 20	24.5 ± 0.70	0.93 ± 0
TAM 40	38 ±15.55*	1.34 ± 0.54*
TAM 60	31.5 ± 4.94*	1.17 ± 0.16
NC	12.25 ± 4.03[a]	0.44 ± 0.12[a]
PC	28 ± 1*	1.06 ± 0.07

NC: Negative Control; PC: Positive Control.
* Statistical difference from NC ($p \leq 0.05$)
[a] Statistical difference from PC ($p \leq 0.05$)
Values are given mean ± SD

Authors' contributions
Experimental planning, design and conducting: Binnaz Kırbıyık, Birgül Mazmancı, Kasım Ocakoğlu.
Writing, original draft preparation: Şeyma Gülnaz Yarlılar, Naz Uğur.
Review of the drafted manuscript: Binnaz Kırbıyık, Birgül Mazmancı, Şeyma Gülnaz Yarlılar, Naz Uğur, Kasım Ocakoğlu.

Declaration of interests
The authors declare that there is no conflict of interests regarding the publication of this paper.

References
Allen TM. 2002. Ligand-targeted therapeutıcs in anticancer therapy. Nat Review Cancer. 2(10): 750-763.

Andres NC, Sieben JM, Baldini M, Rodriguez CH, Famiglietti A, Messina PV. 2018. Electroactive Mg^{2+}-Hydroxyapatite Bender CM, Sereika SM, Brufsky AM, Ryan CM, Vogel VG, Rastogi P, Cohen SM, Casillo FE, Berga SL. 2007. Memory impairments with adjuvant anastrozole versus tamoxifen in women with early-stage breast cancer. Menopause. 14: 995-998.

Blanco E, Shen H, Ferrari M. 2015. Principles of nanoparticle design for overcoming biological barriers to drug delivery. Nature Biotech. 33(9): 941-951.Nanostructured Networks against Drug-Resistant Bone Infection Strains. ACS Appl Mater Interfaces.

Bora DK, Rozhkova EA, Schrantz K, Wyss PP, Braun A, Graule T. Costable EC. 2012. Functionalization of Nanostructured Hematite Thin-Film Electrodes with the Light-Harvesting Membrane Protein C-Phycocyanin Yields an Enhanced Photocurrent. Adv Func Mat. 22: 490–502.

Carlson RW, Hudis CA, Pritchard KI. 2006. Adjuvant endocrine therapy for hormone receptor-positive breast cancer: Evolution of NCCN, ASCO, and St Gallen Recommendations. J Nat Comp Cancer Network. 4(10): 971-979.

Çavaş T. 2011. In vivo genotoxity evauation of atrizine and atrizine-based herbicide on fish Carassiu auratus using the micronucleus test and the comet assay. Food Chem Tox. 49: 1431-1435.

Fisher B, Costantino JP, Wickerham DL, Redmond CK, Kavanah M, Cronin W M, Vogel V. Robidoux A, Dimitrov N, Atkins J, Daly M, Wieand S, Tan-Chiu E, Ford L, Wolmark N. 1998. Tamoxifen for prevention of breast cancer: report of the National Surgical Adjuvant Breast and Bowel Project P-1 Study. J Nat Cancer Ins. 90: 1371–1388.

Garcia SN, Gutierrez L, McNulty A. 2013. Real-time cellular analysis as a novel approach for in vitro cytotoxicity testing of medical device extracts. J Biomed Mater Res A. 101: 2097-2106.

Greenlee RT, Hill-Harmon MB, Murray T, Thun M. 2001. Cancer statistics. CA Cancer J for Clin. 51(1): 15-36.

Haley B, Frenkel E. 2008. Nanoparticles for drug delivery in cancer treatment. Urologic Oncology: Seminars and Original Investigations. 26: 57–64.

Han L, Park SW, Park D. 2009. Silica grafted imidazolium-based ionic liquids: efficient heterogeneous catalysts for chemical fixation of CO_2 to a cyclic carbonate. Energy Env Sci. 2: 1286–1292.

Hassan F, Mohammed G, Gamal A, El-Hiti GA, Alshanon A, Yousif E. 2018. Cytotoxic effects of tamoxifen in breast cancer cells. J Unexplored Med Data. 3 (3): 2-9

Hench LL, J. Wilson J. 1993. An Introduction to Bioceramics. World Scientific Publishing Co. 139-189.

Jafari S, Adibkia K. 2014. Application of Hydroxyapatite Nanoparticle in the Drug Delivery Systems. J Mol Phar Org Pro Reserch. 03: 01.

Huang H, Du M, Chen J, Zhong S, Wang J. 2020. Preparation and characterization of abalone shells derived biological mesoporous hydroxyapatite microspheres for drug delivery. Mat. Sci Eng C Mater Biol Appl. 113:110969. doi.org/10.1016/j.msec.2020.110969

Khadka NK, Cheng X, Ho CS, Katsaras J, Pan J. 2015. Interactions of the anticancer drug tamoxifen with lipid membranes. Biophys J. 108 (10): 2492-2501.

Lai W, Chen C, Ren X, In-Seop L, Jiang G, Kong X. 2016. Hydrothermal fabrication of porous holl9ow hydroxyapatite microspheres for a drug delivery system. Mat Sci Eng C. 62: 166–172.

Lazarević SS, Janković-Častvan IM, Jokić BM, Janaćković DT, Petrović RD. 2015. Sepiolite functionalized with N-(3(trimethoxysilyl)propyl)-ethylenediamine triacetic acid trisodium salt, Part I: Preparation and characterization, J Serb Chem Soc. 80(9): 1193–1202.

Maeda H, Wu J, Sawa T, Matsumura Y, Hori K. 2000. Tumor vascular permeability and the EPR effect in macromolecular therapeutics: a review. J Cont Rel. 65(1–2): 271–284.

Maji R, ShekharDey N, Satapathy BS, Mukherjee B, Mondal S. 2014. Preparation and characterization of Tamoxifen citrate loaded nanoparticles for breast cancer therapy. Inter J Nanomed. 9: 3107–3118.

Melo MT, de Oliveria IM, Grivicich I, Guecheva TN, Saffi J, Henriques JAP, Rosa RM. 2013. Diphenyl diselenide protects cultured MCF-7 cells against tamoxifen-induced oxidative DNA damage. Biomed Pharma. 67(4): 329–335.

Mondal S, Dorozhkin SV, Pal U. 2018. Recent progress on fabrication and drug delivery applications of nanostructured hydroxyapatite. Nanomed Nanobiotech. 10 (4):1504.

Netz DJA, Sepulveda P, Pandolfelli VC, Spadaro ACC, Alencastre JB, Bentley MVLB, Marchetti JM. 2001. Potential use of gelcasting hydroxyapatite porous ceramic as an implantable drug delivery system, International Journal of Pharmaceutics. 213(1-2): 117-125.

Nosrati H, Rashidi N, Danafar H, Manjili HK. 2017. Anticancer Activity of Tamoxifen Loaded Tyrosine Decorated Biocompatible Fe_3O_4 Magnetic Nanoparticles Against Breast Cancer Cell Lines. J Inorganic and Organomet Poly Mat. 28(3): 1178-1186.

Öztürk E, Karaboğa A, Dokumacı AH, Yerer MB. 2018. Real-time Analysis of Impedance Alterations by the Effects of Vanadium Pentoxide on Several Carcinoma Cell Lines. Turk J Pharm Sci. 15(1): 1-6.

Paganini-Hill A, Clark LJ. 2000. Preliminary assessment of cognitive function in breast cancer patients treated with tamoxifen. Breast Cancer Res Treat. 64(2): 165-7.

Pasinli A. 2004. Biyomedikal alanlarda kullanılan biyomalzemeler. Makine Teknolojileri Elektronik Dergisi. 4: 25-34.

Uskokovic V, Desai TA. 2014. In vitro analysis of nanoparticulate hydroxyapatite/chitosan composites as potential drug delivery platforms for the sustained release of antibiotics in the treatment of osteomyelitis. J Phar Sci. 103(2): 567-579.

Rehman S, Khan K, Mujahid M, Nosheen S. 2016. Synthesis of Nano Hydroxyapatite and its Rapid Mediated Surface Functionalization by Silane Coupling Agent. Mat Sci Eng C Mater Biol Appl. 675–681.

Rocha JHG, Lemos AF. 2005. Hydroxyapatite scaffolds hydrothermally grown from aragonitic cuttlefish bones. J Mater Chem. 15: 5007–5011.

Senapati S, Mahanta AK, Kumar S, Maiti P. 2018. Controlled drug delivery vehicles for cancer treatment and their performance. Signal Transduct Targed Ther. 3:7

Singh SK, SinghS, Lillard JWJr, Singh R. 2017. Drug delivery approaches for breast cancer. Inter J Nanomed. 12: 6205–6218.

Simek P, Klímová K, Sedmidubsky D, Jankovský O, Pumer M, Sofer Z. 2015. Towards graphene iodide: Iodination of graphite oxide. Nanoscale. 7(1): 261-270.

Şener LT, Albeniz G, Dinç B, Albeniz I. 2017. iCELLigence real time cell analysis system for examining the cytotoxicity of drugs to cancer cell lines. Exp Therap Med. 14: 1866-1870.

Taşkın MB, Şahin Ö, Taşkın H, Atakol O, İnal A, Güneş A. 2018. Effect of synthetic nano-hydroxyapatite as an alternative phosphorus source on growth and phosphorus nutrition of lettuce (Lactuca sativa L.) plant. J Plant Nut. 41(9): 1148-1154.

Tice RR, Agurell E, Anderson D, Burlinson B, Hartmann A, Kobayashi H, Miyamae Y, Rojas E, Ryu J-C, Sasaki YF. 2000. Single cell gel/comet assay: guidelines for in vitro and in vivo genetic toxicology testing. Env Mol Mut. 35: 206–221.

Urcan E, Haertel U, Styllou M, Hickel R, Scherthan H, Reichl FX. 2010. Real-time xCELLigence impedance analysis of the cytotoxicity of dental composite components on human gingival fibroblasts. Dent. Mater. 26(1): 51-58.

Wozniak K, Kolacinska A, Blasinska-Morawie M, Morawiec-Bajda A, Morawiec Z, Zadrozny M, ,Blasiak J. 2007. The DNA-damaging potential of tamoxifen in breast cancer and normal cells. Arch Toxicol. 81:519–527. DOI 10.1007/s00204-007-0188-3

Wu Q, Shi J, Wei J, Yang L, Cao S. 2010. In situ functionalization of hollow mesoporous hydroxyapatite with thermal-responsive on-off gates in supercritical CO_2. Royal Soc Chem. 5(86): 70101-70108.

Yao Y, Zhou Y, Liu L, Xu Y, Chen Q, Wang Y, Wu S, Deng Y, Zhang J and Shao A (2020) Nanoparticle-Based Drug Delivery in Cancer Therapy and Its Role in Overcoming Drug Resistance. Front. Mol. Biosci. 7:193.